RSC Advances

PAPER

Cite this: *RSC Adv.*, 2015, **5**, 27120

Combining superior surface enhanced Raman scattering and photothermal conversion on one platform: a strategy of ill-defined gold nanoparticles

Shuai Liu,[a] Xi Ling,[a] Chengcheng Zhou,[ab] Jin Zhang,[a] Jianbin Huang*[a] and Yun Yan*[a]

Received 5th February 2015
Accepted 11th March 2015

DOI: 10.1039/c5ra02267c

www.rsc.org/advances

We report a facile one-pot strategy of "ill-defined gold nanoparticles (ID-GNPs)" to prepare dual functional gold nanoparticles. The ID-GNPs were prepared in a simple way by tuning the morphology of the regular GNPs with a tiny amount of cetyltrimethyl ammonium bromide (CTAB). The prepared ID-GNPs comprise both quasi-spherical and elongated gold nanoparticles, which allow the presence of coarse surfaces and high density of hot spots. The substrates fabricated with ID-GNPs show dramatic Raman enhancement for *p*-aminothiophenol (PATP). PATP can be detected even at a concentration of 10^{-12} mol L^{-1}. Meanwhile, these ID-GNPs can efficiently convert absorbed photons into heat when irradiated with 808 nm laser. The temperature of the ID-GNPs dispersion can be enhanced 26.0 °C within 10 minutes, which is capable of inducing the phase transition of a temperature-sensitive supramolecular system. Our study suggests that with the strategy of 'ill-defined gold nanoparticles', these two different functionalities can be achieved on one platform.

Introduction

Surface-enhanced Raman spectroscopy (SERS) has drawn considerable attention due to its wide application in chemical and biological detections.[1–4] Materials that exhibit SERS effect often have 'hot spots' resulting from coupled electromagnetic fields.[5–8] For this reason, various gold or silver nanostructures, such as nanorods,[9] nanostar,[10] nanopopcorn,[11] and nanoflower,[12] have been prepared to fabricate SERS substrates. However, these SERS substrates are prepared with complicated procedures which make it difficult for practical application. In this regard, preparation of NPs with high SERS activity in a simple way is highly desired.

Meanwhile, the photothermal conversion effect of gold nanoparticles (GNPs) has also attracted intensive attention, since GNPs undergo rapid nonradiative thermal relaxation which can efficiently convert the absorbed photons into heat.[13] This heat is expected to be utilized in photothermal (PT) therapy if the surface plasmon resonance (SPR) occurs in the near-infrared (NIR) region.[14,15] It is found that GNPs used in PT therapy should have anisotropic structures.[9,16,17] However, so far, it is difficult to prepare GNPs exhibiting both SERS and PT performance.

Considering that the main bottleneck for fabrication of GNPs with SERS and PT dual functions lies in the different needs for their morphologies, we proposed to synthesize ill-defined gold nanoparticles (ID-GNPs). This strategy does not aim at elegantly controlling the morphology of the GNPs. It is expected that the obtained ID-GNPs will have rough surfaces, which lead to high density of hot spots for superior SERS performance. Meanwhile, the ID-GNPs are also anisotropic, so that they may also exhibit photothermal conversion ability.

In this work, we report the fabrication of ID-GNPs by modifying the shape of regular GNPs with commercially available surfactant CTAB. It is well known that the competition between adsorption and desorption of CTAB on different planes of GNPs will lead to the formation of anisotropic GNPs.[18,19] We show that upon controlling the amount of CTAB, ID-GNPs can be formed. The thin films fabricated with ID-GNPs indeed exhibit superior SERS performance. The probe molecule PATP (*p*-aminothiophenol) can be identified even at the concentration of 10^{-12} mol L^{-1}. In addition, the ID-GNPs can convert the photo energy into heat when irradiated with 808 nm laser. The temperature of the ID-GNPs aqueous dispersion can be increased from 24.2 °C to 50.2 °C within 10 minutes, which is capable of inducing the phase transition of the temperature-sensitive SDS@2β-CD supramolecular system. Since these ID-GNPs were prepared in one step at ambient temperature, our strategy provides a simple way to fabricate dual functional GNPs.

[a]*Beijing National Laboratory for Molecular Sciences (BNLMS), State Key Laboratory for Structural Chemistry of Unstable and Stable Species, College of Chemistry and Molecular Engineering, Peking University, Beijing 100871, P. R. China*

[b]*College of Chemistry and Chemical Engineering, Xinjiang University, Urumqi, 830046, P. R. China*

This journal is © The Royal Society of Chemistry 2015

Experimental sections

Materials

The tetradecyldimethyl amine oxide (C_{14}DMAO, Clariant) aqueous solutions with the concentration of 30 wt% were freeze-dried and then recrystallized five times from acetone. Cetyltrimethyl ammonium bromide (CTAB) was prepared by reactions of 1-bromododecane and the trialkylamine, followed by recrystallizing five times from ethanol–acetone. The purities of the surfactants were examined by the lack of minima in their surface tension curves. Hydrochloroauric acid tetrahydrate ($HAuCl_4 \cdot 4H_2O$, Alfa Aesar, 99.9%) and *p*-aminothiophenol (PATP, Sigma-Aldrich, 97%) were used as received. Ultrapure water was used throughout the work. All the other chemicals (A.R. Grade) were purchased from Beijing Chemical Co.

Preparation of ID-GNPs

In a typical procedure, 3.0 mL of 100.0 mM C_{14}DMAO and 220.0 mM C_6OH solution was maintained at 25 °C for hours. Then 45 μL of 10.0 mM CTAB was added with intensive vortex mixing. Later, 62.1 μL of 100.0 mM $HAuCl_4$ was added. After intensive vortex mixing, the mixture was kept under static conditions in a thermostat container at 25.0 ± 0.5 °C. If not specific mentioned, the reduction reaction was performed for 3 days. The intensity of the SPR band in the system was used to monitor the reaction process. The completion of reduction reaction can be indicated by the saturation of UV-Vis absorption. Then the GNPs in solution were collected by centrifugation and washed with ultrapure water for several times.

Characterization of ID-GNPs

The GNPs were characterized with transmission electron microscopy (TEM, JEM-CX100, 80 kV and JEM-2100, 200 kV), scanning electron microscopy (SEM, Hitachi S4800, 10 kV), X-ray diffraction (XRD, Rigaku Dmax-2000, Ni-filtered Cu K_α radiation) and ultraviolet-visible (UV-Vis) spectrophotometer UV-1800 (SHIMADZU). For TEM and SEM measurements, the obtained products were washed with water for 3 times then dispersed in water and dropped onto 230 mesh copper grids coated with carbon film and a silicon wafer, respectively, followed by drying in air at room temperature. For XRD measurements, drops of GNP samples were put on clean glass slide. For UV-Vis measurements, the well-dispersed GNPs in pure water were used.

Raman measurement

Raman spectra measurements were carried out on a Horiba-Jobin Yvon Labram HR800 instrument with a 632.8 nm He–Ne laser. A 100× objective ($N_A = 0.90$) was used to focus the laser beam. The diameter of laser beam focused on the samples was 1 μm. To avoid the disturbance on the GNPs and the probe molecules, a low power laser of 0.34 mW was used to probe the surfaces. The exposure time was 10 s. The spectra for the comparison were obtained under the same conditions. For a typical preparation of SERS sample, 2.5 mL pure water was added into 0.5 mL as-prepared GNPs aqueous and condensed to 80 μL by centrifugation, followed by ultrasonic dispersion. The surface-enhanced Raman scattering (SERS) substrate was prepared by dropping 30 μL concentrated dispersion onto the Si (111) wafer, which was allowed to dry naturally in air. Then the Si wafer covered with the GNPs thin film was immersed into a PATP solution in ethanol (1 mL) for 1 h and dried in the dark at room temperature, which was rinsed with pure water and absolute ethanol several times to remove the free PATP molecules followed by drying in air. In addition, a Si wafer covered with gold particles was prepared by directly reduction of 4 mM $HAuCl_4$ with 35 mM ascorbic acid as the control experiment. The reaction was completed within 30 min.[20] The obtained gold particles were applied as the SERS substrate in a similar way.

SERS enhancement factor calculation

To calculate the empirical enhancement factor, the Raman spectrum of solid PATP on the glass slide was conducted as a reference. The Raman spectrum of PATP on glass substrate is so weak that we have to use a strong laser power of 1.0 mW to get detectable signal. The diameter of laser beam focused on the samples (D) was 1 μm. The exact transmission depth of the laser into the sample (h) was calculated using eqn (1), where λ is the excitation wavelength (nm), n is the refractive index of the surrounding media (air), and N_A is the numerical aperture.[21]

$$h = \frac{n\lambda}{{N_A}^2} \quad (1)$$

Upon inserting $n = 1$, $\lambda = 633$ nm, and $N_A = 0.90$, the value of h is calculated as $h = 7.81 \times 10^{-7}$ m.

The illuminated volume (V) is determined by the penetration depth of the laser into the sample (h) and the illuminated area (A), $V = h \times A = h \times \pi\left(\frac{D}{2}\right)^2$, then the N_{NRS} can be calculated as $N_{NRS} = n_{NRS}N_A = \frac{\rho V}{M_r}N_A$

The enhancement factor (EF) is defined as eqn (2), where I_{SERS} and I_{NRS} are the SERS and the normal Raman intensity, respectively, and N_{SERS} and N_{NRS} are the corresponding number of molecules probed in the SERS Raman measurements.[22]

$$\mathrm{EF} = \frac{I_{SERS}/N_{SERS}}{I_{NRS}/N_{NRS}} \quad (2)$$

The Raman shift at 1078 cm^{-1} is chosen for comparison. For the normal Raman spectrum of PATP (with a density of 1.18 g cm^{-3}), I_{NRS}/N_{NRS} gives a value of 3.2×10^{-7} count (molecule per s per mW)$^{-1}$. For the SERS spectrum of 1 pM PATP, the I_{SERS}/N_{SERS} value was obtained to be 2.6×10^4 count (molecule per s per mW)$^{-1}$, assuming a homogeneous distribution of PATP across the substrate with the diameter 3.5 mm. The enhancement factor (EF) of about 8.1×10^{10} is obtained based on the above data.

Photothermal conversion performance measurement

To measure the photothermal conversion performance of GNPs and of the reference water, 808 nm NIR laser was delivered

through a quartz cuvette containing aqueous dispersion (2.0 mL) of GNPs with concentration of 0.20 mg mL^{-1}, and the light source was equipped with an external adjustable power. The output power was found to be 1.6 W. A thermocouple with an accuracy of ±0.1 °C was inserted into GNPs aqueous solution perpendicular to the path of the laser. The temperature was recorded once per 30 s. In addition, the photothermal conversion effect of the ID-GNPs was applied to induce the temperature-sensitive aggregates transition. First, the ID-GNPs in solution were collected by centrifugation and washed with ultrapure water for several times. Then ID-GNPs were added to a 5.0 mL 10 wt% SDS@2β-CD supramolecular system, where the molar ratio between SDS (sodium dodecyl sulfate) and β-CD is 1 : 2. The final concentration of the GNPs was 0.2 mg mL^{-1}. The mixture was measured as described above.

Results and discussion

Preparation and characterization of ID-GNPs

The gold nanoparticles were prepared in the mixed system of the zwitterionic surfactant tetradecyldimethyl amine oxide (C_{14}DMAO), *n*-hexanol (C_6OH) and $HAuCl_4$, where C_{14}DMAO and C_6OH were used as the reducing agents. To prepare ID-GNPs, different amount of cetyltrimethyl ammonium bromide (CTAB) was added. Fig. 1 and 2 shows the SEM and TEM images of the GNPs, respectively, in the presence of various amount of CTAB. It is found that regular quasi-spherical GNPs with average diameter of 30 nm were produced without and with 0.10 mM CTAB. The morphology of the GNPs becomes ill-defined in the presence of 0.15–0.30 mM CTAB. Plate-like gold particles occur at higher CTAB concentrations, and giant plates of micrometers become dominant at 5 mM CTAB. For comparison, the normalized UV-Vis spectra of the GNPs prepared at various CTAB concentrations are shown in Fig. 3. For the quasi-spherical GNPs (Fig. 3a and b), a single strong plasmon band cantered at 533 nm is observed. In contrast, for the plate-like gold particles (Fig. 3e and f), the plasmon band becomes very broad, which may originate from the overlap of different dipole resonances.[23] It is worth noting that the characteristic plasmon for the ID-GNPs occurs as well, but it extends to the near infrared region (Fig. 3c and d). For the systems with 0.00–0.30 mM CTAB, the plasmon bands near 533 nm are red-shifted, which indicates the size of the GNPs being larger. It is noticed that the plasmon absorption of the ID-GNPs obtained in the 0.15 mM CTAB is broader than that in the 0.30 and 0.50 CTAB system, suggesting the surface of the ID-GNPs in the 0.15 mM CTAB is coarser.[24,25] This is confirmed by the SEM (Fig. 1) and TEM (Fig. 2) observations. The images in these two figures show that plate-like GNPs occurred in the latter two systems, which become dominant as the concentration of CTAB amount to 5 mM. In fact, the electron diffraction patterns in Fig. 2 also reveal this tendency. Selected area electron diffraction (SAED) patterns (insets of Fig. 2) reveal that the spherical (a) and ID-GNPs (c) are polycrystalline, whereas the plate-like GNPs (f) are monocrystalline. However, the SEAD pattern for the ID-GNPs (inset in Fig. 2c) is discrete, which is not as typical as other polycrystalline structures. This means the surface of the ID-GNPs are rather coarse.[26]

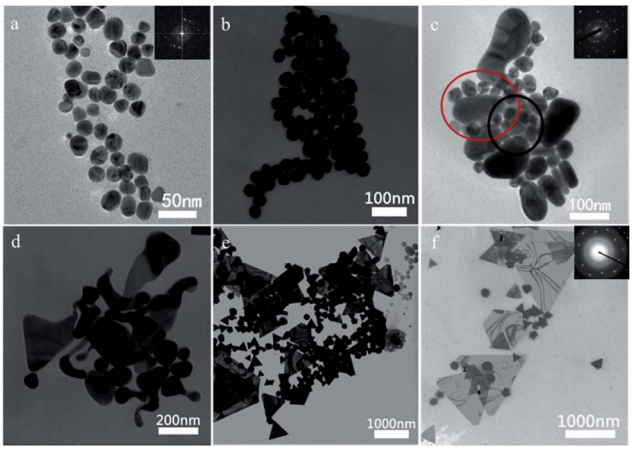

Fig. 2 TEM images of GNPs prepared in the presence of various concentrations of CTAB (a) 0.00, (b) 0.10, (c) 0.15, (d) 0.30, (e) 0.50 and (f) 5.00 mM. The solid circles indicate the core–satellite clusters.

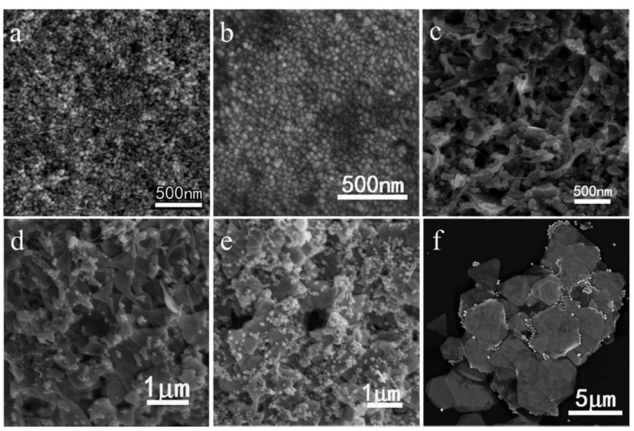

Fig. 1 SEM images of GNPs prepared in the presence of various concentrations of CTAB (a) 0.00, (b) 0.10, (c) 0.15, (d) 0.30, (e) 0.50, and (f) 5.00 mM.

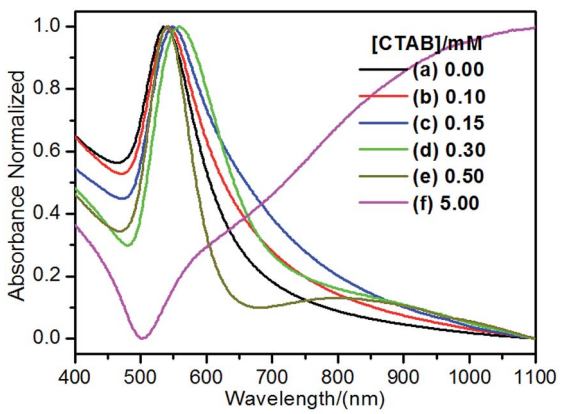

Fig. 3 Normalized UV-Vis spectrum of GNPs prepared in the presence of various concentrations of CTAB: (a) 0.00, (b) 0.10, (c) 0.15, (d) 0.30, (e) 0.50 and (f) 5.00 mM.

This journal is © The Royal Society of Chemistry 2015

Fig. 4 shows the XRD patterns for the GNPs. Four sharp reflections corresponding to the (111), (200), (220), and (311) planes were observed for all the GNPs, suggesting that these GNPs all adopt face-centred cubic (fcc) structure (JCPDS no. 04-0784). It is well known that the addition of CTAB will facilitate the formation of plates due to its strong adsorption on the (111) plane of gold.[18,27] In all the patterns, the intensity of the peak corresponding to the (111) plane is the strongest. Usually, the intensity ratio of the (200) and the (111) diffraction is used to characterize the fraction of the (111) plane in the GNPs.[28] The less the ratio of (200)/(111) is, the more (111) planes there are.[29,30] The (200)/(111) ratios for the 0.00, 0.10, 0.15, and 0.30 mM CTAB systems are 0.33, 0.35, 0.14 and 0, respectively. Obviously, the (111) plane becomes dominant with increasing the concentration of CTAB.

SERS activity of ID-GNPs

To test the SERS activity of the ID-GNPs, PATP was used as the probe molecule.[31] A thin layer of the ID-GNPs was deposited on a silicon wafer to serve as SERS substrate. In addition, control experiments were made on the silicon wafer covered with GNPs prepared by direct reduction of $HAuCl_4$ with ascorbic acid.[20] It is found that the SERS intensity on the ID-GNPs thin film prepared in the presence of 0.15 and 0.30 mM CTAB is remarkably stronger than that on others (Fig. 5). It is noticed that the strongest SERS signal occurs in the 0.15 mM CTAB system, which is about 10 times of that obtained on the directly reduced GNP films. The SERS intensity decreases sharply as the size of the ID-GNPs increases.

It is widely accepted that the SERS intensity is a combination effect of chemical enhancement and electromagnetic enhancement (EM). Usually, EM enhancement is dominant,[32–35] since the surface plasmon may produce very strong electromagnetic fields after excitation. Compared with the Raman spectrum of PATP on glass, the Raman shift on gold substrates is changed and the Raman intensity is significantly enhanced, suggesting the occurrence of chemical bonding between the thiol group in PATP and the surface of the GNPs.[36] Since the chemical enhancement can be considered similar in all the systems in this study, we anticipate it is the EM enhancement contribution determines the final SERS intensity. It is noticed in the TEM observations that the ID-GNPs have clustered into core–satellite structures (Fig. 2b). Similar results were reported to show strong localized SPR which induces the enhancement of Raman intensity.[37] Moreover, the coarse surface of the ID-GNPs also contributes significantly to the EM effect. The local core–satellite structures together with the coarse surfaces in the 0.15 mM CTAB system are thus the dominating structural factors that allow the super strong EM effect in this study.

As a substrate exhibiting SERS activity, it is very relevant to detect its SERS sensitivity. For this reason, the silica wafer covered with the ID-GNPs prepared in the presence of 0.15 mM CTAB was used as SERS substrate to measure the Raman spectra of PATP at different concentrations. Fig. 6 shows that the characteristic Raman peaks can still be identified as the concentration of PATP is decreased to 1.0 pM. Under such conditions, the local enhancement factor (EF) was estimated to be larger than 8.1×10^{10} (see the Experimental sections for details). This extremely high EF value indicates that the ID-GNPs are indeed very effective in producing super strong SERS signals.

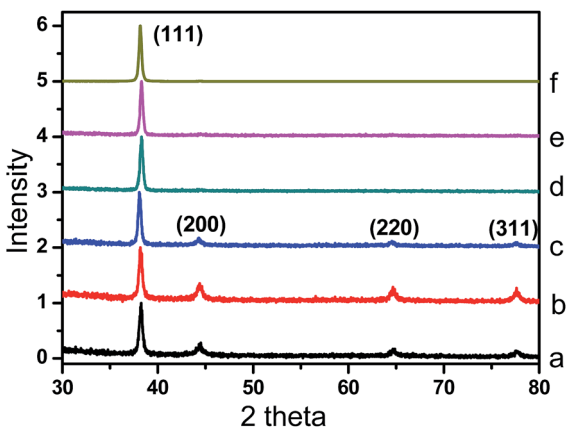

Fig. 4 X-ray diffraction patterns (XRD) of GNPs prepared in the presence of various concentrations of CTAB: (a) 0.00, (b) 0.10, (c) 0.15, (d) 0.30, (e) 0.50 and (f) 5.00 mM. The curves are normalized and moved vertically for clarity.

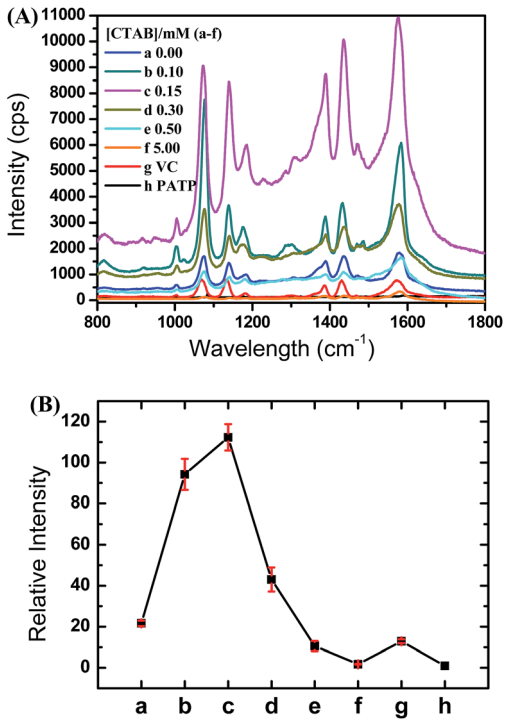

Fig. 5 (A) Raman spectrum of solid PATP (h) and SERS spectra of PATP molecules adsorbed on different substrates, thin films of GNPs obtained at various concentrations of CTAB (a)–(f) and reduction by VC (g). Excitation wavelength: 633 nm; laser power: 0.34 mW; acquisition time: 10 s. (B) The comparison of the mean relative Raman signal intensity at 1078 cm^{-1} obtained on different substrates. Intensity of sample (h) was used as standard.

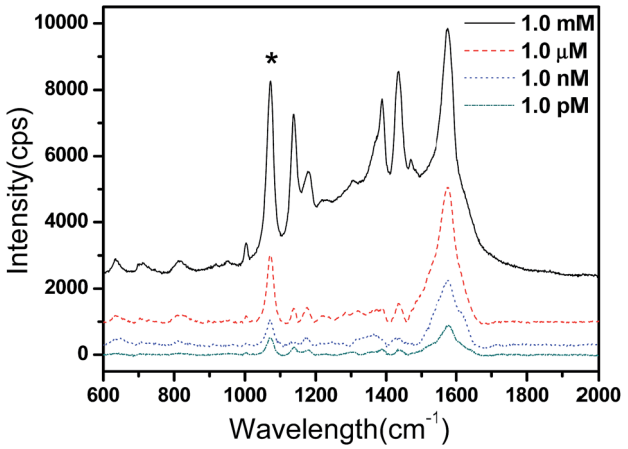

Fig. 6 SERS spectra of different concentrations of PATP adsorbed on ID-GNPs thin films fabricated by ID-GNPs prepared in the presence of 0.15 mM CTAB. Stars indicate characteristic Raman peaks of PATP at 1078 cm^{-1}. The curves are moved vertically for clarity. Excitation wavelength: 633 nm; laser power: 0.34 mW; acquisition time: 10 s.

Photothermal conversion performance of ID-GNPs

It is noticed that the SPR of ID-GNPs has extended to the near infrared region. This suggests that these particles may also exhibit photothermal conversion ability. To verify this, the aqueous dispersion of the ID-GNPs prepared in the presence of 0.15 mM CTAB system was irradiated under the 808 nm laser. It is very striking that the temperature increased from 24.2 °C to 50.2 °C within 10 minutes (see Fig. 7A). Such a huge temperature jump can trigger the tube-vesicle transition in the supramolecular self-assembling system of cyclodextrin/sodium dodecyl sulfate (SDS@2β-CD). In our previous work, we reported that the 2 : 1 inclusion complex of β-CD and SDS can form opalescent and viscoelastic phases which are composed of microtubes at 25 °C.[38] However, the microtubes may transform into vesicles as the temperature increases to 42 °C, which is accompanied by the macroscopic phase transition from opalescent to bluish.[39] From Fig. 7B, it is clearly seen that before irradiation the SDS@2β-CD supramolecular system with ID-GNPs is so turbid that the magneton cannot be observed. However, the turbidity of the system decreases drastically and the magneton on the bottom becomes visible after 10 minutes irradiation under 808 nm laser. This cycle is reversible and can be repeated several times, suggesting the ID-GNPs have excellent photothermal conversion effect. It is known that a temperature above 42 °C is sufficient to kill tumor cells.[40] This means that the strategy of ID-GNPs may have potential medical applications if the size can be adjust to smaller than 100 nm.[41,42]

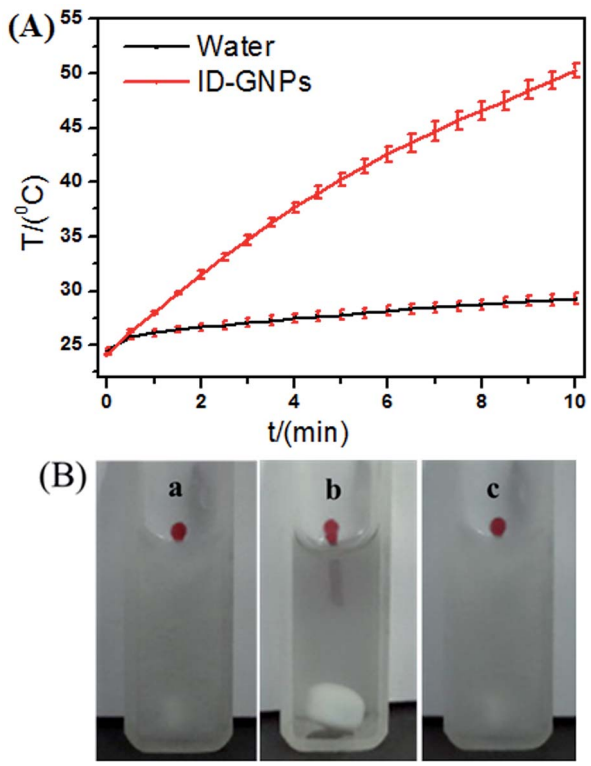

Fig. 7 (A) Mean temperature elevation of pure water and aqueous dispersions of GNPs prepared in the presence of 0.15 mM CTAB. The concentration for the GNPs is 0.2 mg mL^{-1}. The irradiation time is 10 min, and room temperature is 24.2 °C. (B) Phase transition of SDS@2β-CD (10% wt) induced by ID-GNPs under 808 nm irradiation. (a) Before irradiation; (b) after 10 min irradiation; (c) after removal of the laser (5 min later).

Conclusions

In conclusion, we reported a strategy by utilizing ill-defined gold nanoparticles (ID-GNPs) to realize superior SERS performance and photothermal conversion dual functions. The ID-GNPs with rough surface and core–satellite clusters can be easily prepared in the presence of appropriate amount of CTAB. PATP can still be detected even at a concentration of 1 pM on the ID-GNPs. Under the 808 nm irradiation, the ID-GNPs can also increase the temperature of water over 26 °C within 10 minutes. Undoubtedly, the strategy of ID-GNPs provides a new method to combine SERS and photo-thermal dual functions. We expect that by tuning the size of the ID-GNPs to smaller than 100 nm, these ID-GNPs may be used as both SERS imaging and photothermal therapy agent in clinical applications. Work toward this goal is under way in our lab.

Acknowledgements

This work is supported by National Natural Science Foundation of China (Grant no. 21173011, 21273013), the National Basic Research Program of China (973 Program, 2013CB933800), and Doctoral Program of Higher Education of China. The authors thank Andong Wang for revising the manuscript.

Notes and references

1 M. Fleischmann, P. J. Hendra and A. McQuilla, *Chem. Phys. Lett.*, 1974, **26**, 163–166.
2 M. G. Albrecht and J. A. Creighton, *J. Am. Chem. Soc.*, 1977, **99**, 5215–5217.
3 A. Campion and P. Kambhampati, *Chem. Soc. Rev.*, 1998, **27**, 241–250.

 This journal is © The Royal Society of Chemistry 2015

4 C. R. Yonzon, D. A. Stuart, X. Zhang, A. D. McFarland, C. L. Haynes and R. P. Van Duyne, *Talanta*, 2005, **67**, 438–448.

5 G. Braun, I. Pavel, A. R. Morrill, D. S. Seferos, G. C. Bazan, N. O. Reich and M. Moskovits, *J. Am. Chem. Soc.*, 2007, **129**, 7760–7761.

6 S. J. Lee, A. R. Morrill and M. Moskovits, *J. Am. Chem. Soc.*, 2006, **128**, 2200–2201.

7 J. Zhang, X. Li, X. Sun and Y. Li, *J. Phys. Chem. B*, 2005, **109**, 12544–12548.

8 H. L. Wu, H. R. Tsai, Y. T. Hung, K. U. Lao, C. W. Liao, P. J. Chung, J. S. Huang, I. C. Chen and M. H. Huang, *Inorg. Chem.*, 2011, **50**, 8106–8111.

9 G. von Maltzahn, A. Centrone, J. H. Park, R. Ramanathan, M. J. Sailor, T. A. Hatton and S. N. Bhatia, *Adv. Mater.*, 2009, **21**, 3175–3180.

10 C. G. Khoury and T. Vo-Dinh, *J. Phys. Chem. C*, 2008, **112**, 18849–18859.

11 W. Lu, A. K. Singh, S. A. Khan, D. Senapati, H. Yu and P. C. Ray, *J. Am. Chem. Soc.*, 2010, **132**, 18103–18114.

12 Q. Li, Y. Y. Jiang, R. C. Han, X. L. Zhong, S. Y. Liu, Z. Y. Li, Y. L. Sha and D. S. Xu, *Small*, 2013, **9**, 927–932.

13 A. O. Govorov and H. H. Richardson, *Nano Today*, 2007, **2**, 30–38.

14 H. T. Ke, J. R. Wang, Z. F. Dai, Y. S. Jin, E. Z. Qu, Z. W. Xing, C. X. Guo, X. L. Yue and J. B. Liu, *Angew. Chem., Int. Ed.*, 2011, **50**, 3017–3021.

15 S. Jung, J. Nam, S. Hwang, J. Park, J. Hur, K. Im, N. Park and S. Kim, *Anal. Chem.*, 2013, **85**, 7674–7681.

16 X. Huang, I. H. El-Sayed, W. Qian and M. A. El-Sayed, *Nano Lett.*, 2007, **7**, 1591–1597.

17 C.-L. Peng, Y.-H. Shih, P.-C. Lee, T. M.-H. Hsieh, T.-Y. Luo and M.-J. Shieh, *ACS Nano*, 2011, **5**, 5594–5607.

18 X. He, X. J. Zhao, Y. X. Chen and J. Y. Feng, *Mater. Charact.*, 2008, **59**, 380–384.

19 S. H. Chen and D. L. Carroll, *Nano Lett.*, 2002, **2**, 1003–1007.

20 Y. Qiao, H. F. Chen, Y. Y. Lin and J. B. Huang, *Langmuir*, 2011, **27**, 11090–11097.

21 R. A. Alvarez-Puebla, *J. Phys. Chem. Lett.*, 2012, **3**, 857–866.

22 J. B. He, X. M. Lin, R. Divan and H. M. Jaeger, *Small*, 2011, **7**, 3487–3492.

23 Q. T. Zhao, L. S. Hou, C. J. Zhao, S. P. Gu, R. Huang and S. H. Ren, *Laser Phys. Lett.*, 2004, **1**, 115–117.

24 J. Rodriguez-Fernandez, A. M. Funston, J. Perez-Juste, R. A. Alvarez-Puebla, L. M. Liz-Marzan and P. Mulvaney, *Phys. Chem. Chem. Phys.*, 2009, **11**, 5909–5914.

25 Y. M. Zhai, J. F. Zhai, Y. L. Wang, S. J. Guo, W. Ren and S. J. Dong, *J. Phys. Chem. C*, 2009, **113**, 7009–7014.

26 A. Grigore, S. Spallek, A. Petschelt, B. Butz, E. Spiecker and U. Lohbauer, *Dent. Mater.*, 2013, **29**, 1098–1107.

27 C. J. Murphy, T. K. San, A. M. Gole, C. J. Orendorff, J. X. Gao, L. Gou, S. E. Hunyadi and T. Li, *J. Phys. Chem. B*, 2005, **109**, 13857–13870.

28 P. Kannan and S. A. John, *Nanotechnology*, 2008, **19**, 085602.

29 Y. G. Sun and Y. N. Xia, *Adv. Mater.*, 2003, **15**, 695–699.

30 W. L. Huang, C. H. Chen and M. H. Huang, *J. Phys. Chem. C*, 2007, **111**, 2533–2538.

31 Y. F. Huang, H. P. Zhu, G. K. Liu, D. Y. Wu, B. Ren and Z. Q. Tian, *J. Am. Chem. Soc.*, 2010, **132**, 9244–9246.

32 J. Gersten and A. Nitzan, *J. Chem. Phys.*, 1980, **73**, 3023–3037.

33 K. Kneipp, Y. Wang, H. Kneipp, L. T. Perelman, I. Itzkan, R. Dasari and M. S. Feld, *Phys. Rev. Lett.*, 1997, **78**, 1667–1670.

34 J. Jiang, K. Bosnick, M. Maillard and L. Brus, *J. Phys. Chem. B*, 2003, **107**, 9964–9972.

35 M. Moskovits, *Rev. Mod. Phys.*, 1985, **57**, 783–826.

36 T. Wang, X. G. Hu and S. J. Dong, *J. Phys. Chem. B*, 2006, **110**, 16930–16936.

37 N. Gandra, A. Abbas, L. M. Tian and S. Singamaneni, *Nano Lett.*, 2012, **12**, 2645–2651.

38 L. X. Jiang, Y. Peng, Y. Yan, M. L. Deng, Y. L. Wang and J. B. Huang, *Soft Matter*, 2010, **6**, 1731–1736.

39 C. Zhou, X. Cheng, Y. Yan, J. Wang and J. Huang, *Langmuir*, 2014, **30**, 3381–3386.

40 G. M. Hahn, J. Braun and I. Harkedar, *Proc. Natl. Acad. Sci. U. S. A.*, 1975, **72**, 937–940.

41 B. D. Chithrani, A. A. Ghazani and W. C. W. Chan, *Nano Lett.*, 2006, **6**, 662–668.

42 H. S. Choi, W. Liu, P. Misra, E. Tanaka, J. P. Zimmer, B. I. Ipe, M. G. Bawendi and J. V. Frangioni, *Nat. Biotechnol.*, 2007, **25**, 1165–1170.

This journal is © The Royal Society of Chemistry 2015